Research Article Vol. 39, No. 9 / September 2022 / Journal of the Optical Society of America B 2387

Journal of the Optical Society of America B

OPTICAL PHYSICS

Wide frequency band expansion of permittivity normal modes

PARRY Y. CHEN,* YAKOV GREENBERG, AND YONATAN SIVAN

School of Electrical and Computer Engineering, Ben-Gurion University, Israel
**Corresponding author: parryyu@post.bgu.ac.il*

Received 9 May 2022; revised 20 July 2022; accepted 24 July 2022; posted 25 July 2022; published 11 August 2022

Normal modes are valuable tools for modeling electromagnetic resonators, since all their electromagnetic properties can be extracted from a small set of modes. To extend the utility of normal modes to open systems, a set of modes was developed where permittivity is designated to be the eigenvalue. However, these modes, also known as generalized normal modes, are defined at only a single frequency, which limits their utility for spectral applications. In this paper, we present a simple way to extend the validity of permittivity modes to neighboring frequencies. This enables the evaluation of spectral lineshapes and scattering of short pulses from open nanophotonic structures using knowledge of the generalized normal modes at only a single frequency.

https://doi.org/10.1364/JOSAB.463341

1. INTRODUCTION

In recent years there has been significant progress in the development of modal techniques for the solution of electromagnetic simulations; these provide concise physical insight into the understanding of scattering of electromagnetic waves, along with increased computation speed. This included the development of efficient normalization techniques for complex frequency modes (known as resonant states [1–3] or quasi-normal modes [4–7]), along with the numerical [8,9] and perturbative [1–3,10,11] techniques needed for computation of their modes. An alternative approach relies on generalized normal modes, for which the eigenvalue is designated to be the permittivity of the scatterer [12–17]; this approach also benefits from numerical [14,18], asymptotic [16,19], and perturbative [11,20] approaches.

These modal approaches have enabled the study of a range of complex physics and/or computationally intensive problems in electrodynamics and nano-optics, such as strong coupling, superradiance and Fano resonances [7], light scattering in disordered media and random lasing [7,13], the Purcell effect [7,21,22], Förster energy transfer [21], complex quantum electrodynamic effects [23], magnetism, chirality and bi-anisotropy [24,25], metal photoluminescence [26], nonlinear optics [27], thermal emission [28], etc.

Despite the various mathematical complications associated with complex frequency quasi-normal modes (see discussion in [14]), they seem to enjoy much wider use relative to complex permittivity normal modes. The probable reason is that the former enable spectral lineshapes to be obtained in a straightforward manner, whereas permittivity normal modes can obtain lineshapes only by repeated simulation over all frequencies within the range of interest.

In this paper, we develop an approach to overcome this limitation of generalized normal modes and demonstrate an efficient way of extending the applicability of each permittivity mode to a broad range of frequencies. In Section 2, we develop a Taylor-expansion based formulation to derive the permittivity modes over a range of frequencies from the known modes at a single frequency. In Section 3, we implement the formulation to study the scattering of a short electromagnetic pulse from configurations of individual and multiple wires. We demonstrate good accuracy versus exact simulations and much shorter computational speed compared with multiple simulations, often required for Green's tensor calculations, performed with standard commercial software [29]. In Section 4, we conclude and discuss potential future developments. We anticipate that the approach described in this work will precipitate the widespread adoption of generalized normal mode expansions for the study of nanophotonic systems.

2. FORMULATION

Generalized normal modes, or eigenpermittivity modes, allow the electric field $\boldsymbol{E}(\boldsymbol{r}, k)$ due to a specified impinging field $\boldsymbol{E}_0(\boldsymbol{r}', k)$ on an open optical system to be decomposed in terms of its localized eigenmodes $\boldsymbol{E}_m(\boldsymbol{r}; k)$ [14],

$$\boldsymbol{E}(\boldsymbol{r}, k) = \boldsymbol{E}_0(\boldsymbol{r}, k) + \sum_m \boldsymbol{E}_m(\boldsymbol{r}, k) \frac{\epsilon_i(k) - \epsilon_b}{\epsilon_m(k) - \epsilon_i(k)} \times \int \boldsymbol{E}_m(\boldsymbol{r}', k)^\dagger \theta(\boldsymbol{r}') \boldsymbol{E}_0(\boldsymbol{r}', k) \mathrm{d}\boldsymbol{r}'. \quad (1)$$

Here, $k = \omega/c$ is the free-space wavenumber at a specific frequency ω, $\epsilon_i(k)$ is the inclusion permittivity, and $\epsilon_m(k)$ are

the eigenpermittivities. We have assumed that there is a uniform dispersion-free background permittivity, ϵ_b, and defined $\theta(\boldsymbol{r})$ to be an indicator function defining the shape of the inclusion. Similarly, the Green's tensor $\bar{\bar{G}}(\boldsymbol{r}, \boldsymbol{r}'; k)$ can be decomposed in permittivity modes as

$$\bar{\bar{G}}(\boldsymbol{r}, \boldsymbol{r}'; k) = \bar{\bar{G}}_0(|\boldsymbol{r} - \boldsymbol{r}'|; k) + \frac{1}{k^2} \sum_m \frac{\epsilon_i(k) - \epsilon_b}{(\epsilon_m(k) - \epsilon_i(k))(\epsilon_m(k) - \epsilon_b)} \times \boldsymbol{E}_m(\boldsymbol{r}; k) \otimes \boldsymbol{E}_m^{\dagger}(\boldsymbol{r}'; k), \tag{2}$$

where $\bar{\bar{G}}_0(|\boldsymbol{r} - \boldsymbol{r}'|; k)$ is the Green's tensor of the homogeneous background [30]. The key benefit of Eqs. (1) and (2) is that the variation of $\bar{\bar{G}}(\boldsymbol{r}, \boldsymbol{r}'; k)$ over source $\boldsymbol{r}'$ and detector $\boldsymbol{r}$ coordinates is decomposed into two factors, $\boldsymbol{E}_m(\boldsymbol{r}; k)$, and its adjoint $\boldsymbol{E}_m^{\dagger}(\boldsymbol{r}'; k)$. This means that once the modes have been found, it is then easy to obtain $\bar{\bar{G}}(\boldsymbol{r}, \boldsymbol{r}'; k)$ for any source position and orientation.

However, the modes $\boldsymbol{E}_m(\boldsymbol{r}; k)$ and their associated eigenpermittivities $\epsilon_m(k)$ are only applicable to a single frequency $k = \omega/c$. They are defined by the eigenvalue equation

$$s_m(k) \boldsymbol{E}_m(\boldsymbol{r}; k) = \int G_0(|\boldsymbol{r} - \boldsymbol{r}'|; k) \theta(\boldsymbol{r}') \boldsymbol{E}_m(\boldsymbol{r}'; k) \mathrm{d}\boldsymbol{r}', \tag{3}$$

where the eigenvalue s_m is linked to the eigenpermittivity

$$\frac{1}{s_m(k)} = \frac{\epsilon_m(k) - \epsilon_b}{\epsilon_b}. \tag{4}$$

To obtain $\boldsymbol{E}(\boldsymbol{r}, k)$ and $\bar{\bar{G}}(\boldsymbol{r}, \boldsymbol{r}', k)$ over a range of frequencies, we would need to solve this eigenvalue equation for $\epsilon_m(k)$ and $\boldsymbol{E}_m(\boldsymbol{r}, k)$ over the entire desired frequency range, which can be a computationally expensive task.

One simple way to remedy this issue is to assume that the eigenpermittivities and eigenmodes can be expanded as Taylor series about some central frequency k_0,

$$\epsilon_m(k) = \epsilon_m|_{k_0} + (k - k_0)\partial_k \epsilon_m|_{k_0} + \frac{1}{2!}(k - k_0)^2 \partial_k^2 \epsilon_m|_{k_0} + \frac{1}{3!}(k - k_0)^3 \partial_k^3 \epsilon_m|_{k_0} + \cdots. \tag{5}$$

Calculating the eigenpermittivity at k_0 and its derivatives requires fewer simulations, and is a cost-effective way of obtaining the result over a relatively large frequency range. Similarly, we may expand the eigenmodes as

$$\boldsymbol{E}_m(\boldsymbol{r}, k) = \boldsymbol{E}_m|_{k_0} + (k - k_0)\partial_k \boldsymbol{E}_m|_{k_0} + \frac{1}{2!}(k - k_0)^2 \partial_k^2 \boldsymbol{E}_m|_{k_0} + \frac{1}{3!}(k - k_0)^3 \partial_k^3 \boldsymbol{E}_m|_{k_0} + \cdots. \tag{6}$$

Although third-order terms were displayed in the above equations, a lower-order expansion may suffice for many practical purposes. There are two components of Eqs. (1) and (2) that we do not bother to expand as a Taylor series. First, $\epsilon_i(k)$ is regarded as a known parameter of the system, either from an analytic model or from experimental measurements. We shall also assume that an analytical expression is available for $\bar{\bar{G}}_0(|\boldsymbol{r} - \boldsymbol{r}|, k)$ or that the dependence of $\boldsymbol{E}_0(\boldsymbol{r}, k)$ on frequency is supplied.

Quantitative testing showed that it is preferable not to evaluate the integral in Eq. (1) for every different frequency we may want to consider, so we also choose to expand it as a Taylor series. For notational convenience, we define the integral as

$$\mathcal{I}_m(k) = \int \boldsymbol{E}_m(\boldsymbol{r}, k)^{\dagger} \theta(\boldsymbol{r}) \boldsymbol{E}_0(\boldsymbol{r}, k) \mathrm{d}\boldsymbol{r}, \tag{7}$$

allowing the Taylor expansion

$$\mathcal{I}_m(k) = \mathcal{I}_m|_{k_0} + (k - k_0)\partial_k \mathcal{I}_m|_{k_0} + \frac{1}{2!}(k - k_0)^2 \partial_k^2 \mathcal{I}_m|_{k_0} + \frac{1}{3!}(k - k_0)^3 \partial_k^3 \mathcal{I}_m|_{k_0} + \cdots. \tag{8}$$

To employ the expansions Eqs. (5)–(8), analytic expressions can be obtained for the derivatives of the eigenpermittivities and eigenmodes [31]. Another simple way is to compute the derivatives via finite difference, which we shall use in our implementation.

3. NUMERICAL EXAMPLE

It is highly advantageous to avoid the troublesome step of expanding the modal fields in a Taylor series, Eq. (6). Such expansions are prone to errors, since the fields are oscillatory functions of frequency, for which Taylor series expansions are not ideal. Furthermore, the phase variation of the field becomes increasingly rapid and challenging to expand, as it increases linearly with distance from the scatterers.

Our extensive testing showed that these issues can be avoided to a large extent for many geometries, since the modal fields can be expressed as linear combinations of the known modes of simpler shapes. For example, for scattering from a cluster consisting of more than one cylinder, the modes are not available in analytical form. However, they can be represented using single cylinder modes as a basis, which are known analytically. A treatment of the single cylinder case via Taylor expansion is provided in Appendix A. The multi-cylinder case then builds upon these results, by solving the matrix eigenvalue problem [12,21,32,33]

$$V\boldsymbol{c} = s\boldsymbol{c}, \tag{9}$$

where $\boldsymbol{c}$ is a column vector representing an eigenmode of the cluster expressed as coefficients of the single cylinder modes, s is related to the eigenpermittivity of the cluster mode, and V is a matrix of overlap integrals between the single cylinder modes. This hybridization procedure converges upon the modes for the cluster with arbitrary accuracy, since the single cylinder modes provide a complete basis.

In this case, we may expand the eigenvectors $\boldsymbol{c}$ in lieu of expanding the eigenmodes over all space. This can be achieved

by solving Eq. (9) at several neighboring frequencies and using the finite-difference formulas. The underlying single cylinder eigenmodes also vary as a function of frequency, but this variation can be handled analytically using the methods of Appendix A.

In practice, the task of obtaining the derivatives of $\boldsymbol{c}$ from finite difference is a numerically sensitive procedure. Thus, it is advisable to use an analytical formula for the derivative of an eigenvector. We give the formula in the case of a symmetric V [34],

$$\boldsymbol{c}_m' = \sum_{n \neq m} \boldsymbol{c}_n \frac{\boldsymbol{c}_n \cdot V' \boldsymbol{c}_m}{s_n - s_m}, \tag{10}$$

where the prime indicates differentiation with respect to k. The derivative V' can be obtained reliably via finite differences. It is also possible to obtain higher-order derivatives using increasingly more complex formulas that nevertheless still only require knowledge of V'.

We now present a numerical example, treating a two cylinder cluster, shown in Fig. 1. Figure 2 displays the eigenpermittivities of the modes of the cluster as a function of frequency. In this case, it is necessary to specify the distance separation between the two cylinders, but no orientation is necessary, since modes exist in the absence of any incident fields. The parameters are given in the figure caption. For the purposes of clarity, we choose to show only the six brightest modes.

We observe that the Taylor expansion is accurate over a moderate frequency range, and has some difficulty extrapolating beyond any inflection points. If great accuracy over a wide band is desired, multiple Taylor expansions may be employed to cover the range of interest. Alternatively, a more sophisticated expansion can be used, such as Padé's approximation, which provides better extrapolation beyond these inflection points.

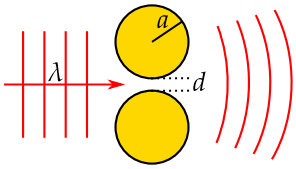

Fig. 1. Schematic of the simulation geometry, where the distance separation is $d/a = 0.2$, measured from the boundary of each cylinder, and a is the radius of each cylinder. When obtaining the modes, no incidence fields are specified. Having obtained the modes, we then use them for the specific direction of the incidence pulse shown.

Having obtained an expansion of the modes and their eigenpermittivity, we proceed to demonstrate a pulse scattering experiment. We continue to use the geometry of Fig. 2, featuring two cylinders separated by a small gap. Figure 3 displays the scattering of a short pulse at various instants in time. The simulation proceeds in two stages. First, the necessary derivatives are calculated, i.e., derivatives for expanding the eigenvalues via Eq. (5), and the integral via Eq. (8). The eigenmodes are represented using the single cylinder basis of Appendix A via Eq. (9), and expanded in frequency via Eq. (10). The entire procedure does not require the simulation domain to be discretized using a grid or mesh. The construction of all the necessary basis modes and their derivatives was completed in ~ 1.5 s in Matlab, on a desktop computer with an Intel Core i5-8500 processor. This involves 136 modes of the two cylinder configuration, constructed from the hybridization of 68 single cylinder modes. These 68 modes range from angular order $m = -8$ until 8 and radial orders 1 to 4.

Subsequently, the solution can be evaluated using Eq. (1) at any arbitrary position or grid of positions and at any frequency within the range of validity. The spatial variation of the scattered fields is known semi-analytically, since it is represented by a linear combination of single cylinder modes. To construct the solution to our desired pulse, the incidence is first constructed in the Fourier domain as described in Appendix B, and each frequency component is fed into Eq. (7) and assembled to obtain both the scattered and total fields. Using this procedure, we obtain good agreement with a direct simulation that does not use Taylor's expansion. See Appendix A for a more quantitative validation.

We would now like to compare the complexities of our approach to finite-difference time-domain (FDTD) simulations. Unfortunately, such a comparison is not straightforward because the complexity of FDTD scales with the product of the number of grid points and time steps, while the complexity in our approach scales with the number of modes cubed [due to the need to solve the eigenvalue problem Eq. (9)], and does not involve any discretization in space or time. Importantly, the number of modes is typically far smaller than the number of grid points, making our approach favorable.

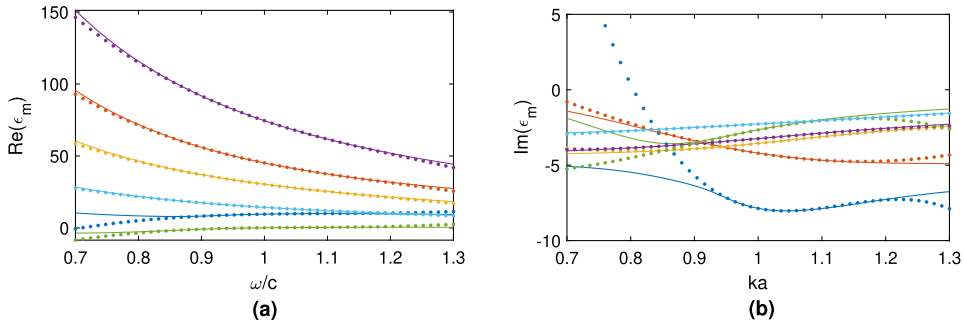

Fig. 2. Real and imaginary parts of eigenpermittivities of several modes as a function of frequency, expressed as the dimensionless quantity $ka = \omega a/c = 2\pi a/\lambda$, where a is the radius of the cylinder. The distance separation is $d/a = 0.2$ (see Fig. 1). Different curves correspond to different modes, showing the six brightest modes. Solid lines were obtained from direct solution of the hybridization equation, Eq. (9), for each separate frequency, while the dots correspond to a Taylor expansion about $ka = 1$.

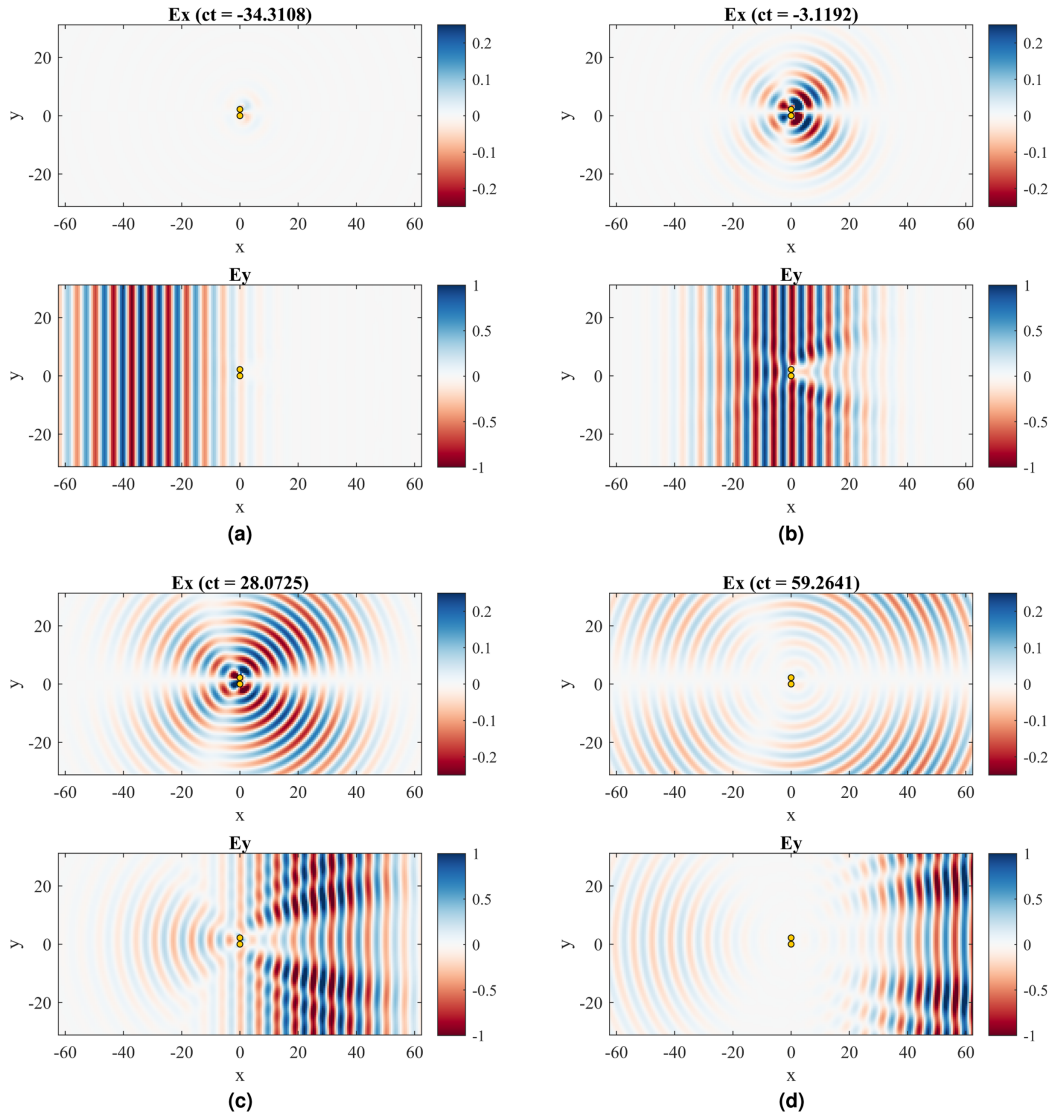

Fig. 3. Results of a pulse scattering experiment where the incident field is traveling from left to right (positive x direction). The electric field component is oriented in-plane (y direction). The parameters of the geometry are the same as in Fig. 2. Additionally, we specify the permittivity of the two cylinders placed at the center of the simulation domain to be $\epsilon_i = 12$, with radius 1 in normalized units. The incident pulse is specified in more detail in Fig. 8. Here, we show the real parts of the E_x and E_y fields. The E_x component is initially zero, but as the pulse approaches and scatters, an E_x component is produced.

Thus, we proceed with a simple comparison. It shows that the simulation times of our approach compare favorably in comparison to FDTD simulation performed on a computer with double the number of cores; considering the high efficiency and low scaling of the latter, this finding is quite encouraging. The commercial package Lumerical required ∼22 s for a dielectric pair of cylinders ($\epsilon = 12$) and ∼70 s for a metallic pair ($\epsilon = -15.2 + 0.4i$). (The Lumerical simulation domain was the same as that of Fig. 3. The simulation grid was generated automatically by Lumerical, with settings auto non-uniform mesh at accuracy 8, with conformal variant 1 mesh refinement. See Lumerical documentation for more details on mesh refinement [35].) We note that these Lumerical run times are for individual simulations, whereas once we have obtained the modes and their derivatives, we can subsequently obtain results for any incidence and any value of inclusion permittivity [14]. This also means that our approach allows easy handling of material dispersion, by simply inputting the desired permittivity at each frequency.

4. SUMMARY AND OUTLOOK

We have developed a frequency expansion of GENOME modes, and demonstrated its implementation for scatterers of relatively simple shapes. This enabled the use of analytic expressions for the modes, obviating the need to expand the modes in a Taylor series [Eq. (6)]. In fact, this procedure can also be applied to scatterers in complex backgrounds (using a simple extension of the technique whereby free-space background is replaced by the Green's tensor of the complex background) and scatterers of arbitrary shape and even non-uniform and anisotropic permittivities, since in general their modes can always be expanded

via a weighted sum of modes of geometries with simple shapes (e.g., of wire modes); see [1–3,11,20,36]. While these perturbative procedures are not as fast as the analytic techniques we used for the simple cylindrical inclusions, they are still significantly faster than commercial mode solvers. Moreover, we emphasize that our approach is most advantageous when repeated simulations are needed (e.g., when computing Green's tensor, performing design optimization, etc.).

Our approach demonstrates how to circumvent the main weakness of generalized normal (permittivity) mode expansions, namely, the need to perform the expansion for each frequency separately. This enables its use for the study of spectral lineshapes and pulse propagation calculations, energy transfer effects from spectrally-wide emitters [21], etc., which can now benefit from the advantages of permittivity mode expansions [14].

APPENDIX A: CONFIRMATION VIA SINGLE CYLINDER SCATTERING

In the special case of a single cylinder, the modes are available analytically once the eigenpermittivity is known. This means that the Taylor expansion, Eq. (6), of the fields is unnecessary. To demonstrate this, we may begin with the known form of two field components within the inclusion interior

$$E_z = \sum_{m,n} C^E_{m,n} J_m(\alpha_{m,n} r) e^{im\theta} e^{i\beta z},$$

$$H_z = \sum_{m,n} C^H_{m,n} J_m(\alpha_{m,n} r) e^{im\theta} e^{i\beta z}, \tag{A1}$$

using the system of coordinates (r, θ, z) and where we now label the modes with indices (m, n) due to the additional symmetry available to the circular cross section. The in-plane propagation constant $\alpha_{m,n}$ is related to the out-of-plane propagation constant β by $\alpha^2 + \beta^2 = \epsilon_{m,n}(k)k^2$. The coefficients $C^{E/H}_{m,n}$ are normalization coefficients that are available analytically [36]. From these two components, all other field components can be derived using Maxwell's equations. Similarly, the modal fields of the background can be related to Eq. (A1) by interfacial jump conditions. In this way, all field components everywhere have a known analytical form based on $\epsilon_{m,n}(k)$, so it is unnecessary to separately store an expansion of the modal field $\boldsymbol{E}_{m,n}(\boldsymbol{r}, k)$. The frequency variation of $\epsilon_m(k)$ can itself be obtained from a transcendental equation known as the dispersion relation or secular equation, e.g., using the efficient and reliable algorithm described in [37].

This analytical form drastically reduces the memory requirements of Taylor expansion. Similarly, if we are considering scattering from a far-field source, the integral in Eq. (7) can be calculated anew for each frequency via an analytical expression. Such computations have negligible cost, and are usually dwarfed by the subsequent evaluation of Eq. (A1) and equivalent expressions for each (r, θ, z) within the simulation domain.

We now provide a numerical example of the single cylinder case, benchmarking the performance of the Taylor expansion against a direct simulation of each frequency via Eq. (1). In Fig. 4, we plot several dispersion relations of eigenpermittivities as a function of ka, where a is the radius of the cylinder. We plot a series of dispersion relations all with angular variation $\exp(i\theta)$, but with different radial orders. This corresponds to $m = 1$ and $n = 1, 2, 3$ in Eq. (A1).

We expanded the dispersion relations via the Taylor series Eq. (5) about $ka = 1$ up to third order. This order is still not computationally expensive to calculate, and is not yet numerically sensitive. Coefficients of the Taylor series were obtained using the central finite-difference formulas. It is seen to approximate well the various dispersion relations, especially in the range from $ka = 0.8$ to 1.2. Some deviations are visible beyond this range, on the order of 3%–4%. This is still acceptable though for many purposes.

The Taylor expansion of the dispersion relation shown in Fig. 4 in principle completes the task of finding $\bar{\bar{G}}(\boldsymbol{r}, \boldsymbol{r}', k)$ as a function of frequency, due to the foregoing discussion that the modal fields are known analytically once the eigenpermittivities are known. However, for completeness, we proceed to demonstrate the use of this expansion in simulating the scattering of a plane wave by a single cylinder at a single frequency, benchmarking against a direct simulation. Figure 5 shows the result computed two different ways, as in Fig. 4. First, the reference calculation is a direct GENOME simulation at $ka = 1.2$. Second, we expand the eigenpermittivity via the Taylor expansion about $ka = 1$, but evaluated at $ka = 1.2$. For the purposes of clarity, only the scattered fields are shown. The fields obtained

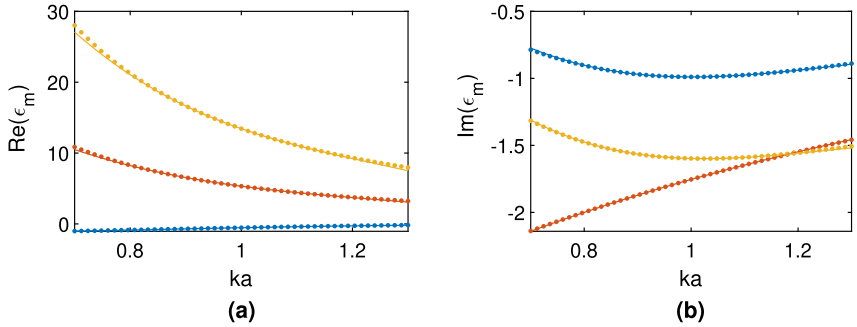

Fig. 4. Real and imaginary parts of eigenpermittivities of modes of a single cylinder as a function of frequency, expressed as the dimensionless quantity $ka = \omega a/c = 2\pi a/\lambda$, where a is the radius of the cylinder. Different curves correspond to different modes, all of azimuthal order $m = 1$ with $e^{im\theta}$ angular variation. Solid lines were obtained from direct solution of the dispersion relation for ϵ_m, and are accurate to numerical precision. Dots correspond to a Taylor expansion of each dispersion relation about $ka = 1$.

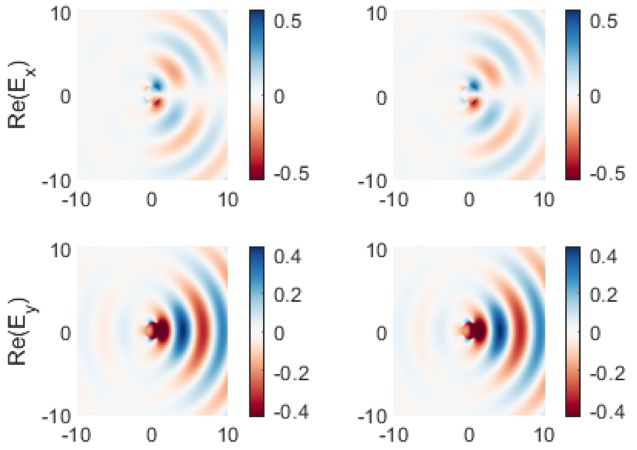

Fig. 5. Comparison of Taylor expansion and direct calculation for a scattering experiment. The incident field is a plane wave with $ka = 1.2$ that is traveling from left to right (positive x direction). The electric field component is oriented in-plane (y direction). A cylinder of permittivity $\epsilon_i = 12$ and radius 1 is placed at the center of the simulation domain. Shown are the real parts of the scattered E_x and E_y fields. The left column displays results calculated directly via GENOME at $ka = 1.2$, while the right column using the Taylor expansion about $ka = 1$ displayed in Fig. 4. Unlike Fig. 4, more modes are used, encompassing all radial orders $n = 1$ to 4 and all angular orders $m = -3$ to 3.

from the Taylor series show excellent agreement with the reference.

To quantify the level of agreement against the reference as a function of ka, we repeat the numerical experiment with different plane wave incidences across the entire range of ka displayed in Fig. 4. Rather than showing the fields, we use the metric

$$\mathrm{Err}^2 = \frac{\int |\boldsymbol{E}_{\mathrm{ref}} - \boldsymbol{E}_{\mathrm{Taylor}}|^2 \mathrm{d}\boldsymbol{r}}{\int |\boldsymbol{E}_{\mathrm{ref}}|^2 \mathrm{d}\boldsymbol{r}}. \tag{A2}$$

We use this metric on the scattered fields only, since the incident field is an input and is identical for both $\boldsymbol{E}_{\mathrm{ref}}$ and $\boldsymbol{E}_{\mathrm{Taylor}}$. In particular, this means we use the scattered field only to compute the denominator $|\boldsymbol{E}_{\mathrm{ref}}|^2$. The domain of integration is over the visible region of Fig. 5. Figure 6 shows this normalized error for each mode of Fig. 4. Roughly speaking, the overall error is constrained by the least accurate mode. We see that the Taylor expansion yields excellent agreement over a wide frequency

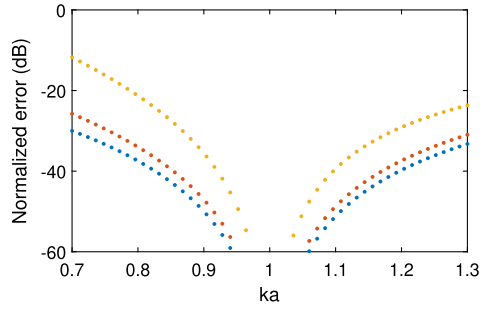

Fig. 6. Normalized error between between GENOME modes and their Taylor expansion over a frequency range for Fig. 5. The error is given by Err in Eq. (A2), and is plotted on a decibel scale. The errors are plotted separately for each mode of Fig. 4, using the parameters described there.

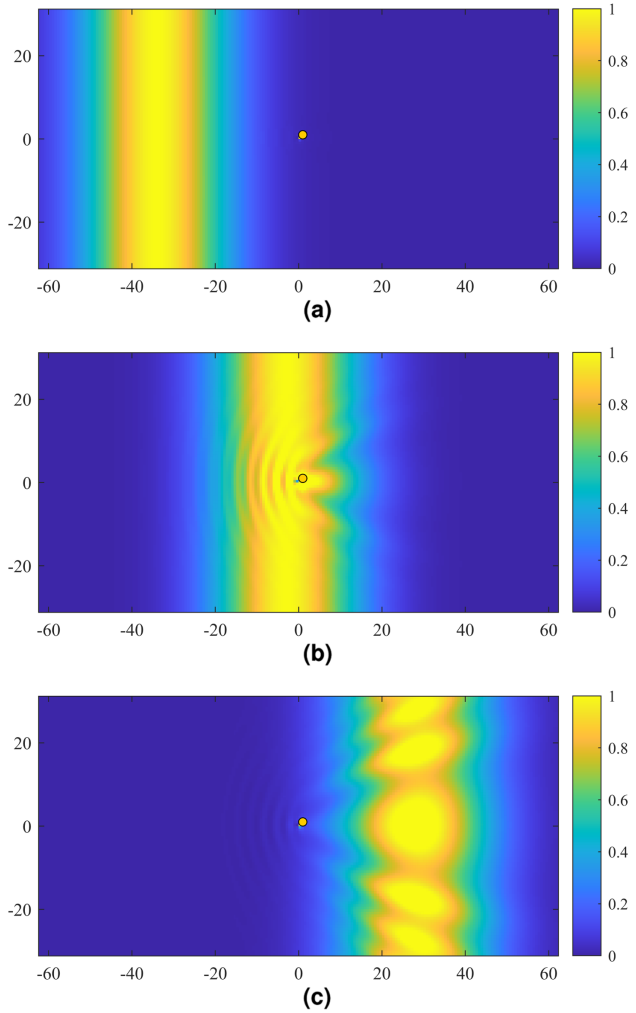

Fig. 7. As with Fig. 5, but showing instead a pulse impinging on a single dielectric cylinder of permittivity 9. The cylinder of radius 1 located at the center of the relatively large visible domain. The intensity of the pulse is displayed, in three snapshots as it travels from left to right and scatters from the cylinder.

range, and is a more than adequate approximation for many numerical purposes.

Finally, we demonstrate the use of the Taylor expanded GENOME in simulating scattering from a pulse, displayed in Fig. 7. We again consider a setup similar to Fig. 5, but with the pulse of Fig. 8 instead of a plane wave. We set the central

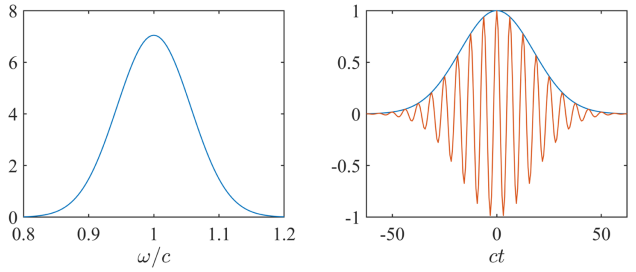

Fig. 8. Pulse used for pulse scattering experiments. The central frequency is $ka = 1$ in normalized units, where a is the cylinder radius, with FWHM of ∼0.1333. In the time domain, this corresponds to a FWHM pulse width of ∼41.5, in normalized units of ct.

frequency of the pulse to $ka = 1$, with $\alpha \approx 1.6 \times 10^{-3}$. This corresponds to a width of ∼0.1333 in the k domain with a pulse width of ∼41.5 (FWHM) in the time domain. Note that the k domain is equivalent to frequency space, since $k = \omega/c$. This means that the vast majority of the energy of the pulse fits within the range of $ka = 0.8$ and 1.2 (which is covered by the Taylor expansion). The Fourier transform was used to synthesize the pulse, using 101 discretization points in k space.

APPENDIX B: FOURIER REPRESENTATION OF PULSES

The expansion of $\bar{\bar{G}}(\boldsymbol{r}, \boldsymbol{r}', k)$ as a function of frequency enables us to simulate scattering from pulses. Suppose the pulse is defined in the time domain by $\boldsymbol{E}_0(\boldsymbol{r}, t)$. We then proceed in the usual way, by first decomposing the pulse into its Fourier components (since the electric field is necessarily a real function, we suppress the need to take the real part of the right-hand side)

$$\boldsymbol{E}_0(\boldsymbol{r}, \omega) = \frac{1}{2\pi} \int_{-\infty}^{\infty} \boldsymbol{E}_0(\boldsymbol{r}, t) e^{i\omega t} \mathrm{d}t. \tag{B1}$$

Each Fourier component is fed into Eq. (1), to obtain the Fourier component of the solution $\boldsymbol{E}(\boldsymbol{r}, k)$. Then the total solution can be composed from these Fourier components:

$$\boldsymbol{E}(\boldsymbol{r}, t) = \int_{-\infty}^{\infty} \boldsymbol{E}(\boldsymbol{r}, \omega) e^{-i\omega t} \mathrm{d}\omega. \tag{B2}$$

In a numerical implementation, we must restrict the domain of integration to a finite range, i.e.,

$$\boldsymbol{E}(\boldsymbol{r}, t) \approx \int_{\omega_1}^{\omega_2} \boldsymbol{E}(\boldsymbol{r}, \omega) e^{-i\omega t} \mathrm{d}\omega, \tag{B3}$$

chosen such that the contribution is negligible outside this range. Second, we must discretize, yielding finally

$$\boldsymbol{E}(\boldsymbol{r}, t) \approx \frac{\omega_2 - \omega_1}{N} \sum_j \boldsymbol{E}(\boldsymbol{r}, \omega_j) e^{-i\omega_j t}, \tag{B4}$$

where N is the total number of discretization points in ω, and ω_j are a set of (equidistant) points that span the domain ω_1 to ω_2.

We shall consider pulses with the Gaussian profile

$$\boldsymbol{E}_0(\boldsymbol{r}, t) = \boldsymbol{E}_0^{(0)} e^{i(\boldsymbol{k}_0 \cdot r - \omega_0 t)} e^{-\alpha t^2}, \tag{B5}$$

where $\boldsymbol{E}_0^{(0)}$ describes the magnitude and polarization of the pulse, $\boldsymbol{k}_0 = \sqrt{\epsilon_b}\omega_0/c$ is the propagation vector, ω_0 is the carrier frequency, and α is related to the pulse width, such that the full width at half maximum is given by $2\sqrt{\log 2/\alpha}$. Its Fourier representation is then

$$\boldsymbol{E}_0(\boldsymbol{r}, \omega) = \frac{1}{2\sqrt{\alpha\pi}} \boldsymbol{E}_0^{(0)} e^{i\boldsymbol{k}_0 \cdot \boldsymbol{r}} e^{-\frac{(\omega-\omega_0)^2}{4\alpha}}. \tag{B6}$$

The FWHM in the Fourier domain is given by $4\sqrt{\alpha \log 2}$.

Funding. Deutsche Forschungsgemeinschaft (WE 5815/5-1).

Acknowledgment. P. Y. C. and Y. S. were partially funded by DFG.

Disclosures. The authors declare no conflicts of interest.

Data availability. Data underlying the results presented in this paper are not publicly available at this time but may be obtained from the authors upon reasonable request.

REFERENCES

1. E. A. Muljarov, W. Langbein, and R. Zimmermann, "Brillouin-Wigner perturbation theory in open electromagnetic systems," Europhys. Lett. **92**, 50010 (2010).
2. M. B. Doost, W. Langbein, and E. A. Muljarov, "Resonant state expansion applied to two dimensional open optical systems," Phys. Rev. A **87**, 043827 (2013).
3. M. B. Doost, W. Langbein, and E. A. Muljarov, "Resonant-state expansion applied to three-dimensional open optical systems," Phys. Rev. A **90**, 013834 (2014).
4. C. Sauvan, J. P. Hugonin, I. S. Maksymov, and P. Lalanne, "Theory of the spontaneous optical emission of nanosize photonic and plasmon resonators," Phys. Rev. Lett. **110**, 237401 (2013).
5. R.-C. Ge, P. T. Kristensen, J. F. Young, and S. Hughes, "Quasinormal mode approach to modelling light-emission and propagation in nanoplasmonics," New J. Phys. **16**, 113048 (2014).
6. W. Yan, R. Faggiani, and P. Lalanne, "Rigorous modal analysis of plasmonic nanoresonators," Phys. Rev. B **97**, 205422 (2018).
7. P. Lalanne, W. Yan, K. Vynck, C. Sauvan, and J.-P. Hugonin, "Light interaction with photonic and plasmonic resonances," Laser Photon. Rev. **12**, 1700113 (2017).
8. Q. Bai, M. Perrin, C. Sauvan, J.-P. Hugonin, and P. Lalanne, "Efficient and intuitive method for the analysis of light scattering by a resonant nanostructure," Opt. Express **21**, 27371 (2013).
9. P. Lalanne, W. Yan, A. Gras, C. Sauvan, J.-P. Hugonin, M. Besbes, G. Demésy, M. D. Truong, B. Gralak, F. Zolla, A. Nicolet, F. Binkowski, L. Zschiedrich, S. Burger, J. Zimmerling, R. Remis, P. Urbach, H. T. Liu, and T. Weiss, "Quasinormal mode solvers for resonators with dispersive materials," J. Opt. Soc. Am. A **36**, 686–704 (2019).
10. T. Weiss, M. Mesch, M. Schäferling, H. Giessen, W. Langbein, and E. A. Muljarov, "From dark to bright: first-order perturbation theory with analytical mode normalization for plasmonic nanoantenna arrays applied to refractive index sensing," Phys. Rev. Lett. **116**, 237401 (2016).
11. P. Y. Chen and Y. Sivan, "Resolving Gibbs phenomenon via a discontinuous basis in a mode solver for open optical systems," J. Comput. Phys. **429**, 110004 (2021).
12. D. J. Bergman and D. Stroud, "Theory of resonances in the electromagnetic scattering by macroscopic bodies," Phys. Rev. B **22**, 3527–3539 (1980).
13. L. Ge, Y. D. Chong, and A. D. Stone, "Steady-state ab initio laser theory: generalizations and analytic results," Phys. Rev. A **82**, 063824 (2010).
14. P. Y. Chen, D. J. Bergman, and Y. Sivan, "Generalizing normal mode expansion of electromagnetic Green's tensor to lossy resonators in open systems," Phys. Rev. Appl. **11**, 044018 (2019).
15. T. Sandu, "Eigenmode decomposition of the near-field enhancement in localized surface plasmon resonances of metallic nanoparticles," Plasmonics **8**, 391–402 (2012).
16. M. S. Agranovich, B. Z. Katsenelenbaum, A. N. Sivov, and N. N. Voitovich, *Generalized Method of Eigenoscillations in Diffraction Theory* (Wiley-VCH, 1999).
17. C. Forestiere and G. Miano, "Material-independent modes for electromagnetic scattering," Phys. Rev. B **94**, 201406 (2016).
18. C. Forestiere, G. Miano, G. Rubinacci, A. Tamburrino, R. Tricarico, and S. Ventre, "Volume integral formulation for the calculation of material independent modes of dielectric scatterers," IEEE Trans. Antennas Propag. **66**, 2505 (2018).
19. O. Schnitzer, "Singular perturbations approach to localized surface-plasmon resonance: nearly touching metal nanospheres," Phys. Rev. B **92**, 235428 (2015).
20. P. Y. Chen, Y. Sivan, and E. A. Muljarov, "An efficient solver for the generalized normal modes of non-uniform open optical resonators," J. Comput. Phys. **422**, 109754 (2020).
21. G. Rosolen, P. Y. Chen, B. Maes, and Y. Sivan, "Overcoming the bottleneck for quantum computations of complex nanophotonic

structures: Purcell and Förster resonant energy transfer calculations using a rigorous mode-hybridization method," Phys. Rev. B **101**, 155401 (2020).
22. G. Rosolen and B. Maes, "Strong multipolar transition enhancement with graphene nanoislands," APL Photon. **6**, 086103 (2021).
23. S. Franke, S. Hughes, M. K. Dezfouli, P. T. Kristensen, K. Busch, A. Knorr, and M. Richter, "Quantization of quasinormal modes for open cavities and plasmonic cavity quantum electrodynamics," Phys. Rev. Lett. **122**, 213901 (2019).
24. E. A. Muljarov and T. Weiss, "Resonant-state expansion for open optical systems: generalization to magnetic, chiral, and bi-anisotropic materials," Opt. Lett. **43**, 1978–1981 (2018).
25. D. J. Bergman, P. Y. Chen, and A. Farhi, "Scattering electromagnetic eigenstates of a two-constituent composite and their exploitation for calculating a physical field," Phys. Rev. A **102**, 063508 (2020).
26. Y. Sivan and Y. Dubi, "Theory of 'hot' photoluminescence from Drude metals," ACS Nano **15**, 8724–8732 (2021).
27. K. N. Reddy, P. Y. Chen, A. I. Fernández-Domínguez, and Y. Sivan, "Revisiting the boundary conditions for second-harmonic generation at metal-dielectric interfaces," J. Opt. Soc. Am. B **34**, 1824–1832 (2017).
28. P. Y. Chen, C. Khandekar, R. Ayash, Z. Jacob, and Y. Sivan, "Thermal emission from non-isothermal nanostructures," Phys. Rev. Appl. **18**, 014052 (2022).
29. Lumerical Solutions, Inc., http://www.lumerical.com/tcad-products/fdtd/.
30. L. Novotny and B. Hecht, *Principles of Nano-Optics* (Cambridge University, 2006).
31. S. Upendar, M. A. Schmidt, and T. Weiss, "What optical fiber modes reveal: group velocity and effective index for external perturbations," J. Opt. Soc. Am. B **38**, 1097–1103 (2021).
32. D. J. Bergman, "Dielectric constant of a two-component granular composite: a practical scheme for calculating the pole spectrum," Phys. Rev. B **19**, 2359–2368 (1979).
33. M. Pascale, G. Miano, R. Tricarico, and C. Forestiere, "Full-wave electromagnetic modes and hybridization in nanoparticle dimers," Sci. Rep. **9**, 14524 (2019).
34. J. Franklin, *Lecture 31, Physics 342* (Reed University, 2008).
35. Lumerical, "Conformal mesh technology details," 2022, https://support.lumerical.com/hc/en-us/articles/360034382614.
36. N. Kossowski, P. Y. Chen, Q. J. Wang, P. Genevet, and Y. Sivan, "Generalized normal modes of an anisotropic scatterer," J. Appl. Phys. **129**, 113104 (2021).
37. P. Y. Chen and Y. Sivan, "Robust location of optical fiber modes via the argument principle method," Comput. Phys. Commun. **214**, 105–116 (2017).